Electronic Supplementary Material (ESI) for Journal of Materials Chemistry C.

Supporting Information

A π-orbital model for substituent effect in organic room-temperature phosphorescent materials

Wenqi Gong[//], Ke Qin[//], Xiaokang Yao, Qiuying Li, Anqi Lv, Wenpeng Ye, Huifang Shi, Zhongfu An, and Huili Ma[*]

Key Laboratory of Flexible Electronics (KLOFE) & Institute of Advanced Materials (IAM), Nanjing Tech University (NanjingTech), 30 South Puzhu Road, Nanjing 211816, China

[//]Wenqi Gong and Ke Qin contributed equally.

AUTHOR INFORMATION

Corresponding Authors

*Huili Ma. E-mail: iamhlma@njtech.edu.cn

Computational and Experimental Methods

Electronic structures. The electronic structures of molecular crystals were performed by using hybrid quantum mechanics/molecular mechanics (QM/MM) theory, including the central QM part and the surrounding MM part modeled by the Universal Force Field (UFF), where a cluster model (5×5×5 supercell) was extracted from X-ray diffraction crystal structure (see Fig. 1). Two-layer ONIOM method was implemented to perform QM/MM calculations using Gaussian 09 package.[1] The electronic embedding is adopted in QM/MM calculations by incorporating the partial charges of the MM region into the quantum mechanical Hamiltonian. The equilibrium configuration and the harmonic vibrational frequency were performed at the level of (TD)O3LYP/def2-SVP, and the nature of low-lying excited states, including excitation energies, spin-orbit coupling (SOC) matrix elements and the natural transition orbitals (NTOs), were then evaluated by using TD-O3LYP/def2-TZVP method. It is worth noting that background charges are not considered when describing NTOs and SOC matrix elements, which were calculated by using quasi-degenerate perturbation theory[2] in ORCA package[3]. For QAT and TX analogs, the fully internally contracted N-Electron Valence State Perturbation Theory (FIC-NEVPT2)[4] was further performed using ORCA software to evaluate the nature of the low-lying excited states, including excitation energies E, oscillator strength f, and SOC matrix elements ξ, together with the active space of 10 electrons in 8 orbitals (10e/8o) for QAT analogs and 6 electrons in 6 orbitals (6e/6o) for TX analogs, as well as def2-SVP basis set. The electrostatic potential (ESP) isosurface was evaluated by using Multiwfn.[5]

Rate constants. The radiative decay rate k_f is estimated by Einstein's spontaneous

emission relationship $k_f = E^2 f \Big/ \left(1.499\ \mathrm{cm}^{-2} \cdot \mathrm{s}\right)$. The rates of decay processes k_{isc}, k_{nr}, and k_{ic} were evaluated by the thermal vibration correlation function rate theory with a Lorentz broadening of 1.0 ps implemented in the MOMAP program.[6] The nonadiabatic coupling is calculated by using TD-B3LYP/def2-SVP method implemented in Turbomole 7.2 program.[7] Noted that Cartesian coordinates are used to calculate the reorganization energy, and the Duschinsky matrix is not involved.

Reagents and materials. All reagents used in the experiments were purchased from commercial sources without further purification.

Measurements. ^{1}H and ^{13}C nuclear magnetic resonance (NMR) spectra were measured with a JOEL NMR spectrometer (JNM-ECZ400S, 400 MHz Japan). Steady-state and delayed photoluminescence spectra were measured using Hitachi F-7100. The photoluminescence lifetimes were collected on an Edinburgh FLS 1000 fluorescence spectrophotometer equipped with a microsecond flash-lamp (μF900), respectively.

Preparation for the phosphors/PVA film. The polymer of PVA-1799 (1.0 g), distilled water (10 mL), phosphors (5.0 mg), and ethanol (1.0 mL) were mixed, heated, and stirred at 373 K for 5 h. Then, the mixed solution (300 μL) was dropped onto a quartz wafer (1.5×1.5 cm^2), which was annealed at 333 K for 12 h. Finally, a transparent film was obtained.

PA-NH_2 was purchased from TCI(Shanghai)Development Co., Ltd. Compound was purified by recrystallization three times with ethyl acetate. ^{1}H NMR (400 MHz, DMSO-d_6): δ 6.00 (s, 2H), δ 6.56 (m, 2H), δ 7.53 (d, J = 8.0 Hz, 2H), δ 12.47 (s, 2H). ^{13}C NMR (101 MHz, DMSO-d_6): δ 170.68, 167.89, 150.78, 137.68, 131.60, 114.89, 112.98, 111.54.

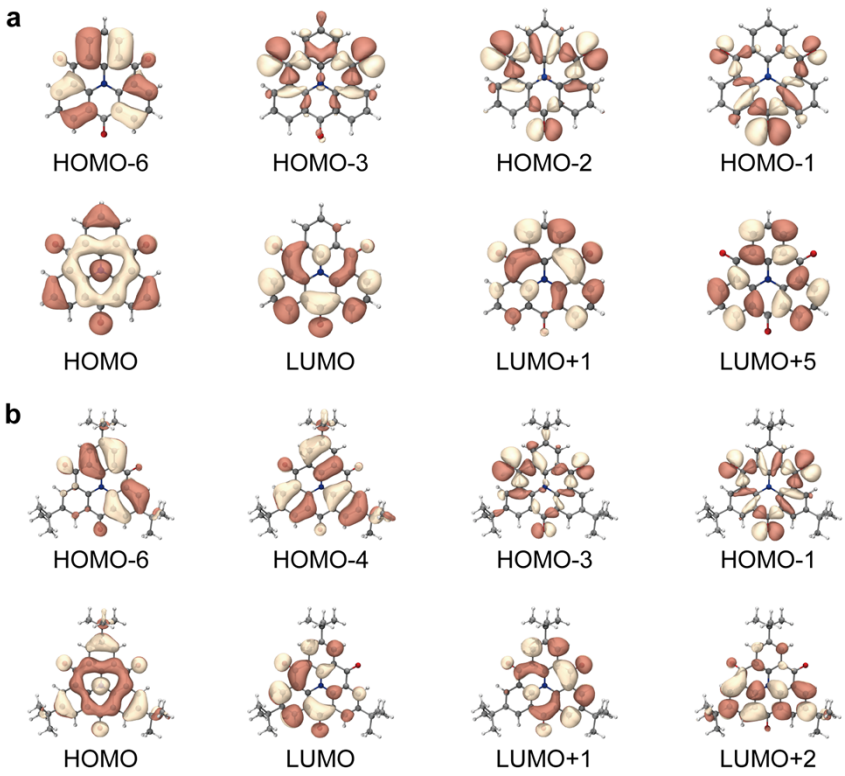

Figure S1. Molecular orbital contour plots within the selected active space for (a) QAT and (b) QAT-*t*Bu.

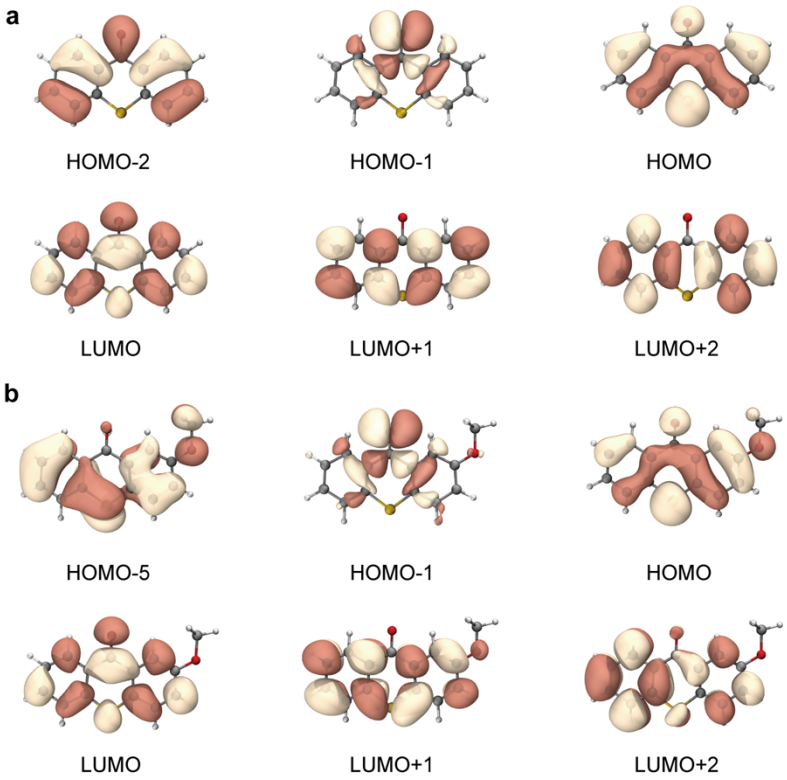

Figure S2. Molecular orbital contour plots within the selected active space for (a) TX and (b) TX-OMe.

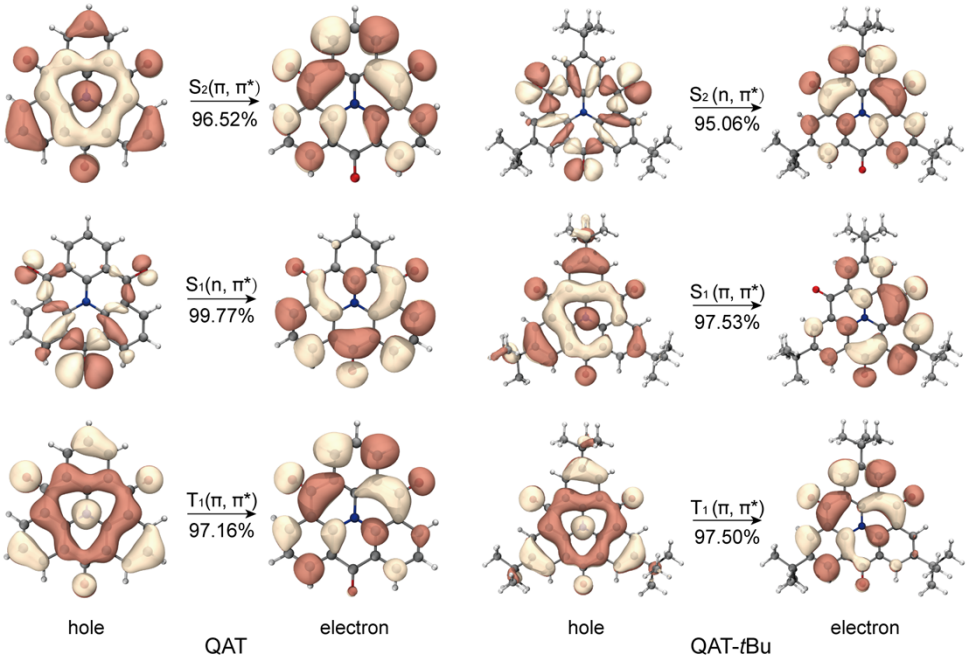

Figure S3. Natural transition orbitals (NTOs) of S_1, S_2 and T_1 states for QAT and QAT-*t*Bu.

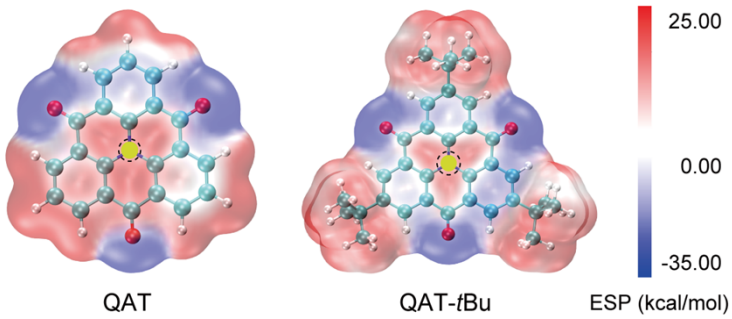

Figure S4. Electrostatic potential surfaces for QAT and QAT-*t*Bu.

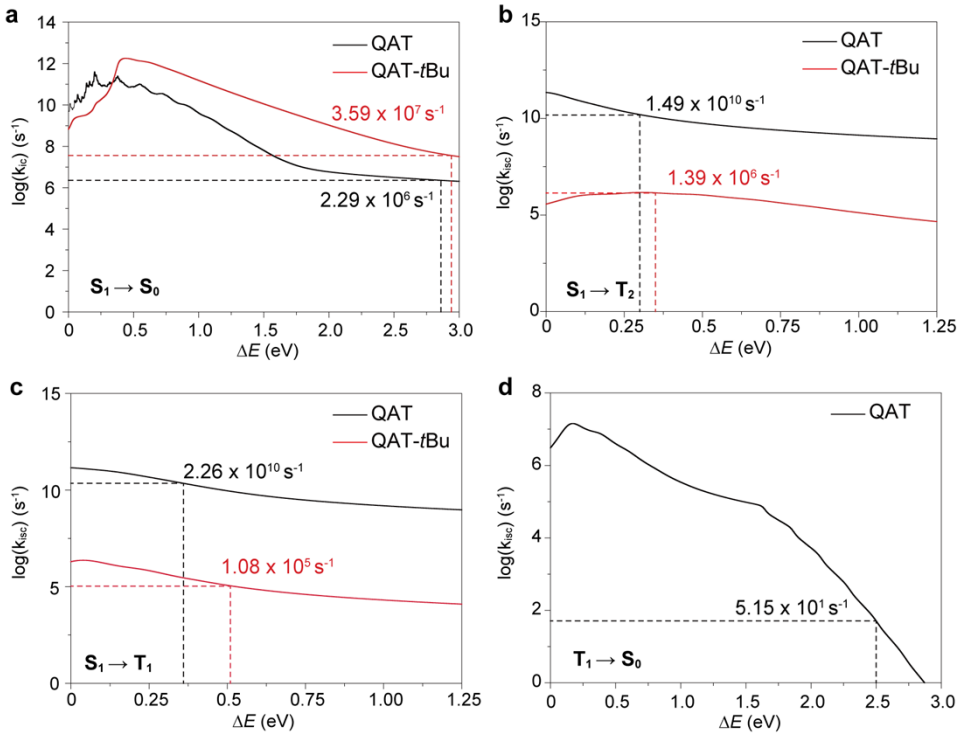

Figure S5. (a) Internal conversion rate (k_{ic}) constant spectra of $S_1 \rightarrow S_0$, and intersystem crossing rate (k_{isc}) constant spectra of (b) $S_1 \rightarrow T_2$ and (c) $S_1 \rightarrow T_1$ for QAT and QAT-*t*Bu, and (d) $T_1 \rightarrow S_0$ for QAT-*t*Bu.

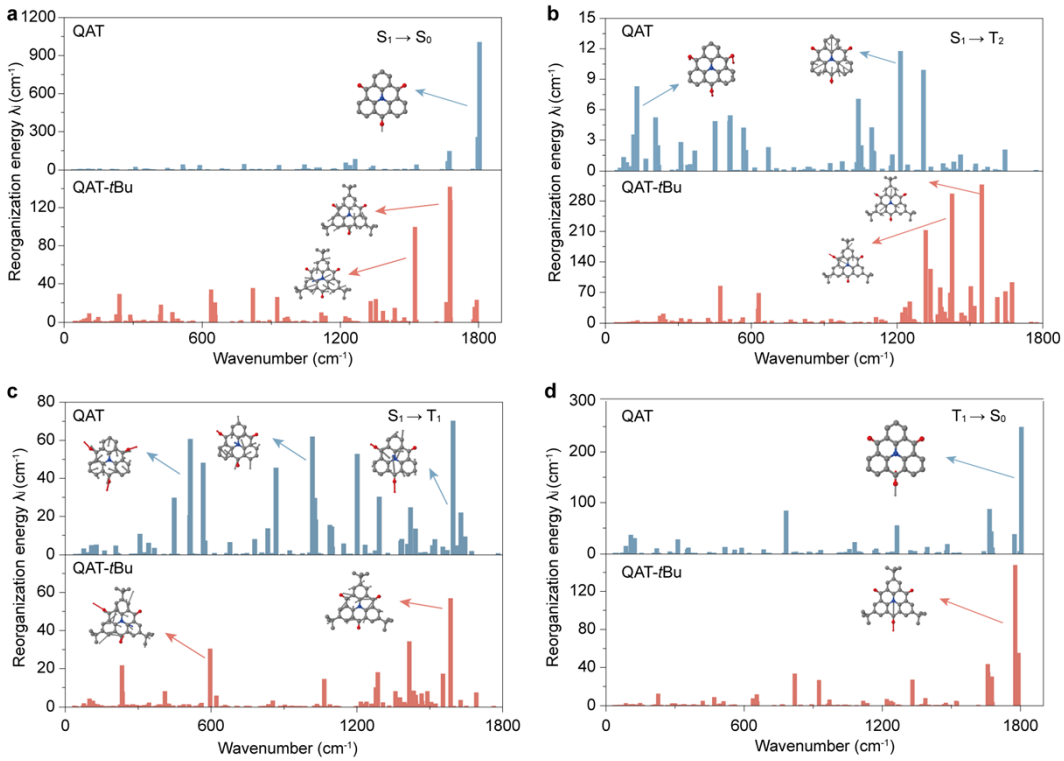

Figure S6. Calculated reorganization energies of (a) $S_1 \rightarrow S_0$, (b) $S_1 \rightarrow T_2$, (c) $S_1 \rightarrow T_1$ and (d) $T_1 \rightarrow S_0$ for QAT and QAT-*t*Bu.

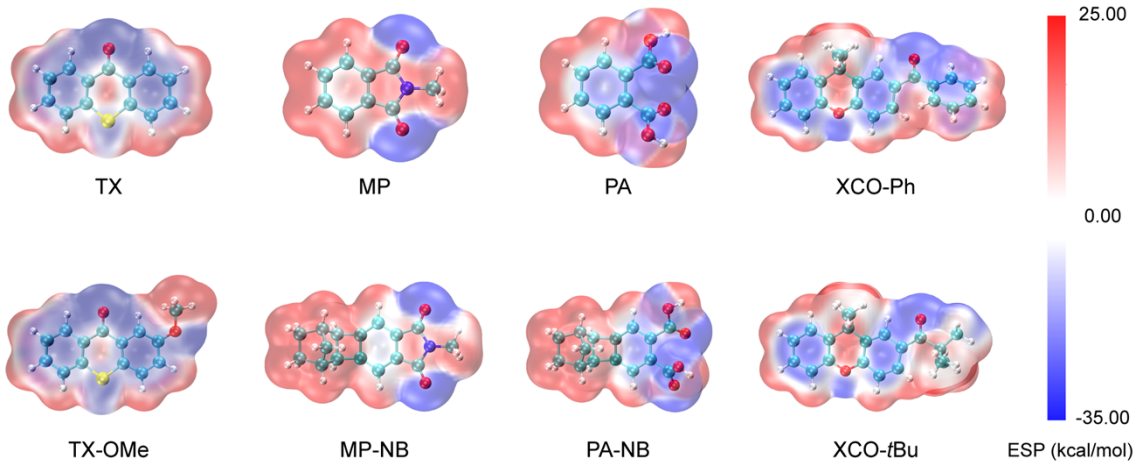

Figure S7. Electrostatic potential surfaces for TX, MP, PA and XCO derivatives.

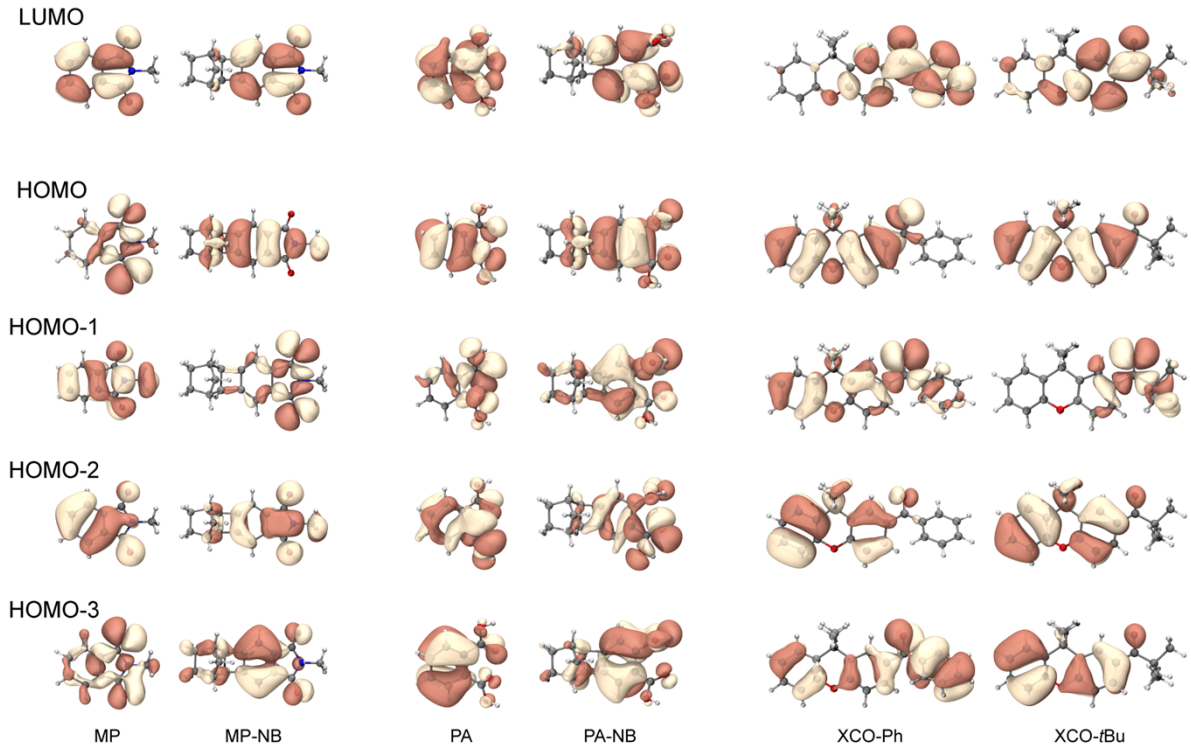

Figure S8. Frontier molecular orbitals (FMOs) for MP, PA and XCO derivatives.

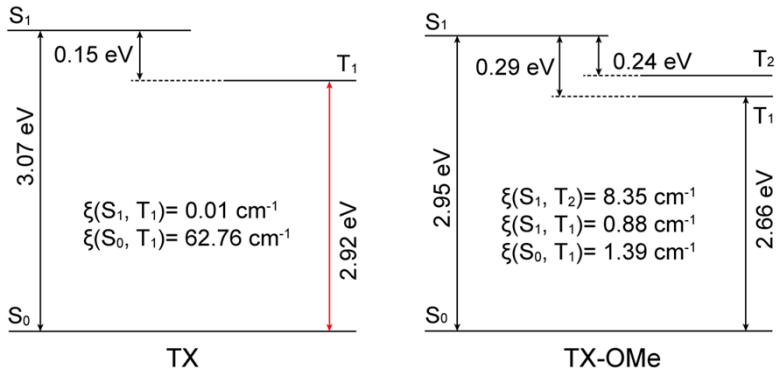

Figure S9. Calculated energy level diagrams and spin-orbit coupling matrix elements (ξ) of the low-lying excited states for TX and TX-OMe at the level of NEVPT2(6e,6o)/def2-TZVP.

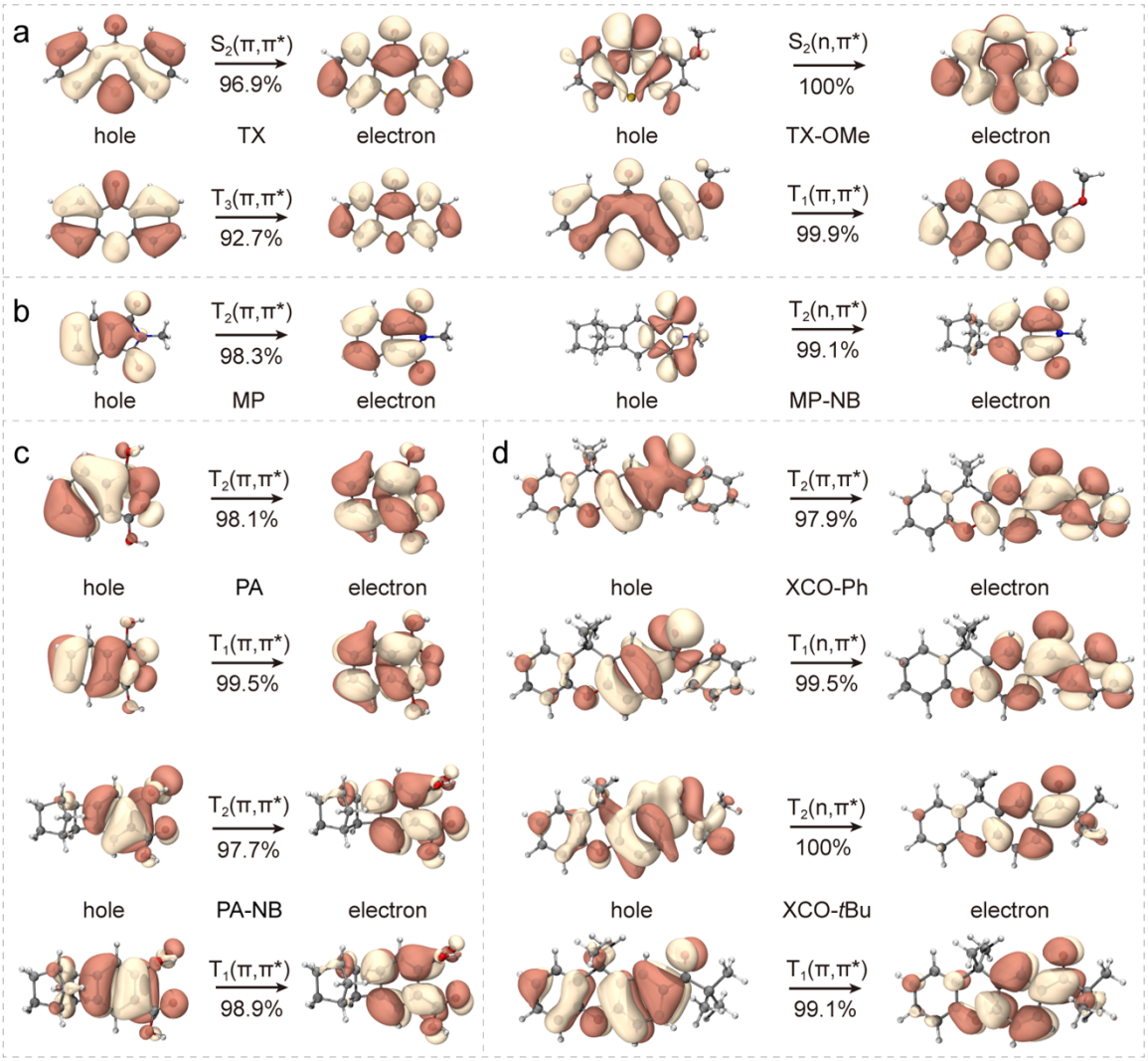

Figure S10. Natural transition orbitals (NTOs) of the low-lying excited states (S_1, S_2, T_1 and T_2) for (a) TX, (b) MP, (c) PA, and (d) XCO derivatives at the TD-O3LYP/def2-TZVP level.

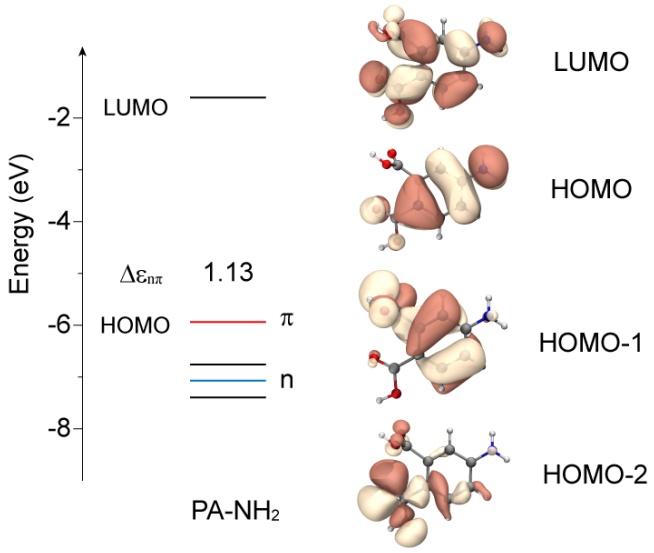

Figure S11. Frontier molecular orbitals of PA-NH2.

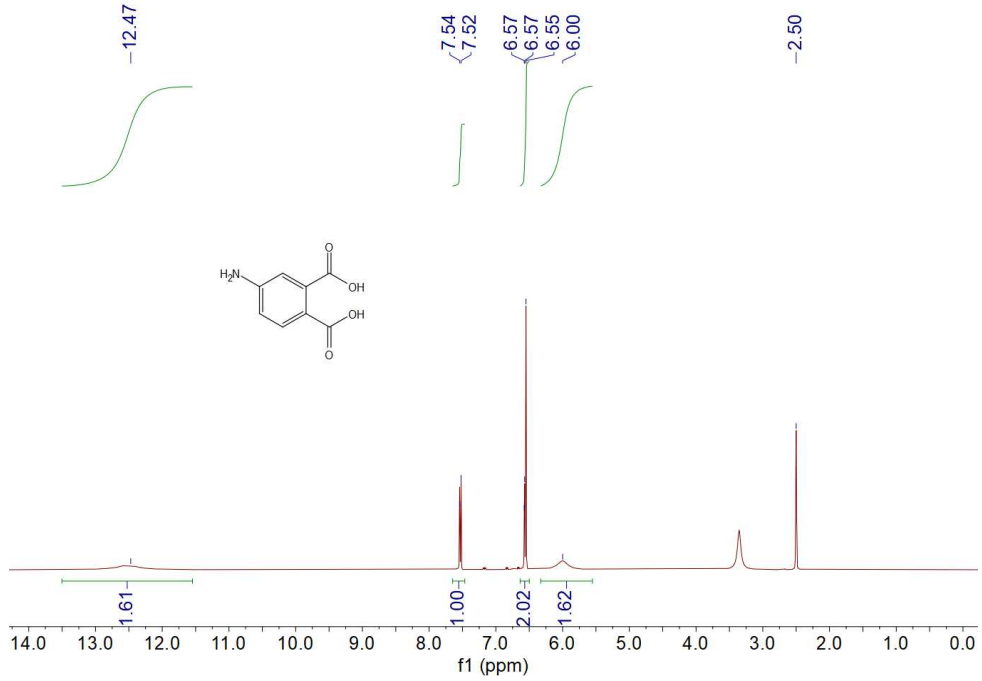

Figure S12. ^{1}H NMR spectrum of PA-NH_2 molecule in DMSO-d_6.

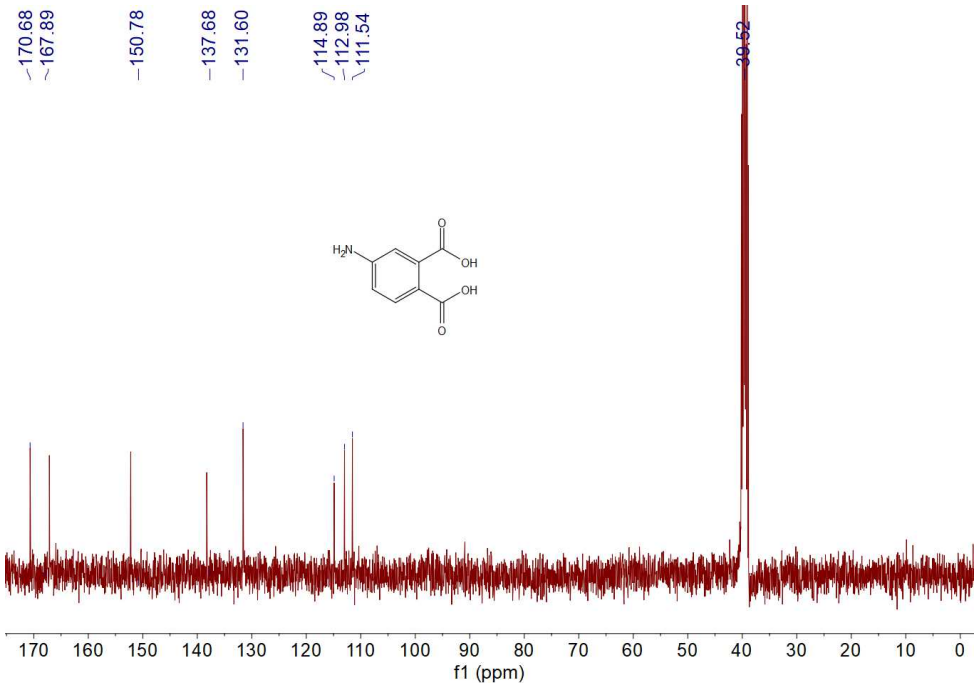

Figure S13. ^{13}C NMR spectrum of PA-NH_2 molecule in DMSO-d_6.

Table S1. Calculated excitation energies (eV) of the low-lying excited states for QAT and QAT-*t*Bu by using NEVPT2 and TD-O3LYP methods, respectively, together with def2-SVP basis sets, based on the S_1-geomtery. The experimental value is shown as a comparison.

States	QAT			QAT-*t*Bu		
	O3LYP	NEVPT2	Exp.	O3LYP	NEVPT2	Exp.
S_1	2.61	2.33	-	2.84	2.40	2.50
T_2	2.33	2.17	-	2.49	2.26	-
T_1	2.28	2.13	2.30	2.37	2.10	-

Table S2. Transition orbitals and components of S_1, T_1 and T_2 for QAT analogs.

Mols.	S_1	T_1	T_2
QAT	H-1 → L (91.8%)	H → L (94.0%)	H → L (86.3%)
QAT-*t*Bu	H → L (96.2%)	H → L (94.4%)	H → L+1 (95.1%)

Table S3. The energy levels (eV) of frontier molecular orbital with and without considering background charges (BGCs) for QAT analogs. $\Delta\varepsilon_{n\pi}$ represents the energy gap between H (π) and H-1 (n), $\Delta\varepsilon_{\pi}$ ($\Delta\varepsilon_{n}$) is the energy gap of π (n) orbital between QAT and QAT-*t*Bu.

	With BGCs (eV)			Without BGCs (eV)		
	H	H-1	$\Delta\varepsilon_{n\pi}$	H	H-1	$\Delta\varepsilon_{n\pi}$
QAT	-6.43	-6.54	0.11	-6.32	-6.40	0.08
QAT-*t*Bu	-5.87	-6.35	0.48	-5.89	-6.34	0.45
$\Delta\varepsilon_{\pi}$	0.56	-	-	0.43	-	-
$\Delta\varepsilon_{n}$	-	0.19	-	-	0.06	-

Table S4. The energy levels (eV) of frontier molecular orbitals for TX, MP, PA, and XCO analogs.

	TX	**TX -OMe**	**MP**	**MP -NB**	**PA**	**PA -NB**	**XCO**	**XCO -*t*Bu**
L+1	-1.44	-1.16	-1.80	-1.53	-1.31	-1.09	-1.01	-0.94
L	-2.61	-2.43	-3.13	-2.92	-2.73	-2.27	-2.43	-2.10
H	-5.84	-5.34	-6.67	-6.31	-6.54	-6.32	-5.57	-5.64
H-1	-6.00	-6.37	-6.96	-6.85	-7.17	-6.94	-6.02	-5.99
H-2	-6.73	-6.65	-7.48	-7.23	-7.26	-7.19	-6.65	-6.68
H-3	-7.06	-6.93	-7.52	-7.36	-7.56	-7.45	-6.78	-6.81

Table S5. The π-electrons components in frontier molecular orbitals for TX, MP, PA, and XCO analogs.

Compound	HOMO	HOMO-1	HOMO-2	HOMO-3
TX	63.41%	0.00%	99.65%	100%
TX-OMe	58.35%	0.27%	71.00%	99.09%
MP	0.00%	89.28	97.81	0.005%
MP-NB	94.43%	0%	91.47%	87.39%
PA	77.13%	2.57%	17.80%	93.58%
PA-NB	87.40%	65.40%	9.06%	82.75%
XCO-Ph	82.87%	21.34%	97.34%	77.40%
XCO-tBu	100%	0.00%	100%	100%

Table S6. Transition orbitals and components of T_1 for MP, PA, and XCO analogs.

Compound	T_1
MP	H→L (98.02%)
MP-NB	H→L (94.69%) H-2→L (2.14%)
PA	H → L (93.00%) H-2 → L (3.98%) H-3 → L+1 (2.07%)
PA-NB	H → L (91.13%) H-1 → L (3.76%)
XCO-Ph	H → L (66.84%) H-1 → L (28.89%)
XCO-tBu	H → L (87.55%) H-2 → L (6.17%) H-3 → L (6.17%)

References

1. M. J. Frisch, G. W. Trucks, H. B. Schlegel, G. E. Scuseria, M. A. Robb, J. R. Cheeseman, G. Scalmani, V. Barone, B. Mennucci, G. A. Petersson, H. Nakatsuji, M. Caricato, X. Li, H. P. Hratchian, A. F. Izmaylov, J. Bloino, G. Zheng, J. L. Sonnenberg, M. Hada, M. Ehara, K. Toyota, R. Fukuda, J. Hasegawa, M. Ishida, T. Nakajima, Y. Honda, O. Kitao, H. Nakai, T. Vreven, J. A. Montgomery, Jr., J. E. Peralta, F. Ogliaro, M. Bearpark, J. J. Heyd, E. Brothers, K. N. Kudin, V. N. Staroverov, R. Kobayashi, J. Normand, K. Raghavachari, A. Rendell, J. C. Burant, S. S. Iyengar, J. Tomasi, M. Cossi, N. Rega, J. M. Millam, M. Klene, J. E. Knox, J. B. Cross, V. Bakken, C. Adamo, J. Jaramillo, R. Gomperts, R. E. Stratmann, O. Yazyev, A. J. Austin, R. Cammi, C. Pomelli, J. W. Ochterski, R. L. Martin, K. Morokuma, V. G. Zakrzewski, G. A. Voth, P. Salvador, J. J. Dannenberg, S. Dapprich, A. D. Daniels, Ö. Farkas, J. B. Foresman, J. V. Ortiz, J. Cioslowski, and D. J. Fox, *Gaussian 09*, *reversion D.01*, Gaussian, Inc., Wallingford, CT, 2009.

2. B. d. Souza, G. Farias, F Neese, R. Izsák, *J. Chem. Theory Comput.*, 2019, 15, 1896-1904.

3. F. Neese, *WIREs Comput. Mol. Sci.*, 2018, 8, e13271.

4. C. Angeli, R. Cimiraglia, J. -P. Malrieu, *J. Chem. Phys.*, 2002, 117, 9138–9153.

5. T. Lu, and F. Chen, *J. Comput. Chem.*, 2012, 33, 580-592.

6. Y. Niu, W. Li, Q. Peng, H. Geng, Y. Yi, L. Wang, *Mol. Phys*., 2018, 116, 1078–1090.

7. TURBOMOLE V7.2 2017, a development of University of Karlsruhe and Forschungszentrum Karlsruhe GmbH, 1989-2007, TURBOMOLE GmbH, since 2007; available from http://www.turbomole.com.